International Journal of Biological Macromolecules 51 (2012) 566–575

Contents lists available at SciVerse ScienceDirect

International Journal of Biological Macromolecules

journal homepage: www.elsevier.com/locate/ijbiomac

Chitosan/halloysite nanotubes bionanocomposites: Structure, mechanical properties and biocompatibility

Mingxian Liu [a], Yun Zhang [a], Chongchao Wu [b], Sheng Xiong [b], Changren Zhou [a,*]

[a] Department of Materials Science and Engineering, Jinan University, Guangzhou 510632, China
[b] Biomedical R&D Center, Guangdong Provincial Key Laboratory of Bioengineering Medicine, National Engineering Research Center of Genetic Medicine, Jinan University, Guangzhou 510632, China

ARTICLE INFO

Article history:
Received 15 May 2012
Received in revised form 12 June 2012
Accepted 14 June 2012
Available online 26 June 2012

Keywords:
Hydrogen bonding
Nanotopography
Fibroblasts

ABSTRACT

Incorporation of nanosized reinforcements into chitosan usually results in improved properties and changed microstructures. Naturally occurred halloysite nanotubes (HNTs) are incorporated into chitosan for forming bionanocomposite films *via* solution casting. The electrostatic attraction and hydrogen bonding interactions between HNTs and chitosan are confirmed. HNTs are uniformly dispersed in chitosan matrix. The tensile strength and Young's modulus of chitosan are enhanced by HNTs. The storage modulus and glass transition temperature of chitosan/HNTs films also increase significantly. Blending with HNTs induces changes in surface nanotopography and increase of roughness of chitosan films. *In vitro* fibroblasts response demonstrates that both chitosan and chitosan/HNTs nanocomposite films are cytocompatibility even when the loading of HNTs is 10%. In summary, these results provide insights into understanding of the structural relationships of chitosan/HNTs bionanocomposite films in potential applications, such as scaffold materials in tissue engineering.

1. Introduction

In the recent years, an extensive interest has arisen in development of products from biobased and renewable resources in view of sustainable development and environmental protection. Chitosan, a linear polysaccharide composed of randomly distributed β-(1-4)-linked D-glucosamine and N-acetyl-D-glucosamine, is a biodegradable and biocompatible polymer which is obtained by alkaline deacetylation of chitin [1]. The chitin is the main component of the exoskeleton of crustaceans and the second most abundant biopolymer in nature after cellulose. Due to its unique structure and property, chitosan is widely used in the field of biomedicine, food package, water treatment, cosmetic and so on [2]. Chitosan can be dissolved in solvents such as dilute aqueous acidic solution and can be processed into films, hydrogels, fibers, porous scaffold [3]. Chitosan films can be obtained by evaporation of solvent from solutions at evaluated temperature or under room temperature. Due to its good biocompatibility and biodegradability, chitosan film is widely used in biomedical and pharmaceutical areas, *i.e.* artificial skin, wound dressing, tissue engineering, and drug carrier [4]. However, the mechanical properties of chitosan film should be improved for these applications. Incorporation of nanosized reinforcements such as hydroxyapatite (HA) [5,6], nanoclay [7,8], carbon nanotubes (CNTs) [9,10], titanium dioxide [11], graphene [12,13] into chitosan can improve the mechanical properties of chitosan. For example, the Young's modulus and ultimate tensile strength of formaldehyde-treated chitosan/HA nanocomposite film containing 66 wt.% (47 vol.%) HA reach up to 17.3 GPa and 222 MPa, respectively, which are significantly higher than those of pure chitosan [6]. With incorporation of only 0.8 wt.% of MWNTs into chitosan, about 93% and 99% increases in tensile modulus and strength have been achieved [9]. Recently, chitosan/graphene nanocomposite films were produced *via* solution casting [12]. With addition of a small amount of graphene (0.1–0.3 wt.%), the elastic modulus of chitosan increases over ~200%. Considering that the amino and hydroxyl groups of chitosan and the positively charged of chitosan in aqueous solution, chitosan can interact with nanoclays *via* hydrogen bonding and/or electrostatic attraction interactions [14,15]. As a consequence, one can blend chitosan with nanoclays in aqueous solution for well dispersed chitosan/clay nanocomposites. Several efforts have been put in to prepare the chitosan/nanoclay composites with improved mechanical and thermal properties [16–19]. The increased interfacial compatibility *via* hydrogen bonding and/or electrostatic attraction between chitosan and clays is responsible for the enhanced performance of the nanocomposites [20,21]. However, most studies only focus on the mechanical reinforcement of chitosan-based nanocomposites. The *in vitro* cytotoxicity

* Corresponding author. Fax: +86 20 8522 3271.
E-mail address: tcrz9@jnu.edu.cn (C. Zhou).

0141-8130/$ – see front matter © 2012 Published by Elsevier B.V.
http://dx.doi.org/10.1016/j.ijbiomac.2012.06.022

evaluation needs to be explored in order to apply these nanocomposites in biomedical field.

Halloysite nanotubes (HNTs) are one-dimensional nanoparticles with hollow nanotubular structure which can be employed for preparing chitosan nanocomposites. HNTs are a kind of layered aluminosilicate with molecular formula of $Al_2Si_2O_5(OH)_4{\cdot}nH_2O$. HNTs belong to the kaolin group of minerals mined from natural deposits [22]. HNTs have an inner diameter of 10–30 nm and an outer diameter of 50–70 nm. The length of HNTs varies in the range of 0.5–1.5 μm. The zeta-potential of HNTs is negative at pH 2–13 due to the surface potential of SiO_2 with a small contribution from the positive Al_2O_3 inner surface [23]. The chemical properties of HNTs' outermost surface are similar to those of SiO_2, while the properties of the inner cylinder core are similar to those of Al_2O_3. HNTs are suitable nanofillers for polymers because of its unique rod-like structure and chemical activities. The addition of HNTs to polymers has shown significant improvement in mechanical and thermal properties [24,25]. Extensive works have been done by our group to investigate the mechanisms of enhancement of mechanical properties in polymer–HNTs nanocomposites [26–30]. However, there have been only a few work on biopolymers and HNTs composites [31–34]. Due to the hydrophilicity of HNTs and the small dimensions, raw HNTs can be readily dispersed in water easily by mechanical stirring or ultrasonic treatment. As a result, they can be solution-mixed with chitosan in aqueous solution for preparing nanocomposite [26]. More importantly, the hydrogen bonding and electrostatic interactions between HNTs and chitosan provide interfacial binding which assist dispersion of the nanotubes. In addition, recent research demonstrates that HNTs are biocompatible which can be used as biomaterials. Vergaro et al. found human epithelial adenocarcinoma cell and breast cancer cell can be adhered, gown and uptaken by HNTs up to concentrations of 75 μg/mL [23]. The polymers/HNTs nanocomposites also showed biocompatibility, such as poly(lactic-co-glycolic acid)/HNTs nanocomposites fibers [35,36] and polyvinyl alcohol/HNTs nanocomposite films [37]. As alternative nanotubes for CNTs, HNTs are availably abundantly, biocompatible and also mechanically strong. Therefore, exploring the effect of HNTs on chitosan is necessary for their low cost and superior performance for biomedical applications.

In present work, chitosan/HNTs bionanocomposite films are prepared *via* solution casting method. The morphological, physical and mechanical properties of the bionanocomposite film are investigated in details. Finally, fibroblasts are cultured on pure chitosan and chitosan/HNTs bionanocomposite films. They are characterized in cell viability assay and cell morphological observation to understand whether the HNTs affect the biocompatibility of chitosan. Due to the high performance and biocompatibility, the prepared chitosan/HNTs bionanocomposites have potential applications in bone tissue engineering and drug carrier systems.

2. Experimental

2.1. Materials

Chitosan was supplied by Jinan Haidebei Marine Bioengineering Co. Ltd. (China). It had a degree of deacetylation of 95% and viscosity-average molecular weight of 600,000 g/mol. The HNTs, were mined from Hunan province, China. The elemental composition by X-ray fluorescence (XRF) was determined as follows (wt.%): SiO_2, 54.29; Al_2O_3, 44.51; Fe_2O_3, 0.63; TiO_2, 0.006. Before using, HNTs were purified according to Ref. [29]. The Brunauer–Emmett–Teller (BET) surface area of the used HNTs was 50.4 m^2/g.

2.2. Preparation of the chitosan/HNTs nanocomposite films

The chitosan/HNTs nanocomposite films were prepared by solution casting method. The typical procedure for preparing the nanocomposite films was described below. 2 g of chitosan was dissolved in 100 ml of 2 wt.% acetic acid solution under mechanical stirring. Then the calculated amount of HNTs was added into the chitosan solution. The mixture solution was continuously stirred overnight and then sonicated for 1 h at ambient temperature to obtain a good dispersion of HNTs. The solution was subsequently poured into a plastic petridish and dried under room temperature to form thin film. The dry film thickness was measured as ~200 μm. HNTs contents in chitosan/HNTs nanocomposites were 2, 5, 7.5 and 10 wt.% and abbreviated as 2%, 5%, 7.5% and 10% in the text. The highest loading of 10% is based on our pervious finding [37]. For comparison, pure chitosan films were also prepared in the same way but without addition of HNTs. All the samples were kept in vacuum desiccator at room temperature before any measurements.

2.3. Physical and mechanical characterizations of pure chitosan and chitosan/HNTs nanocomposites films

2.3.1. UV–vis spectroscopy (UV–vis)

UV–vis transmittance spectra of pure chitosan and chitosan/HNTs bionanocomposite films were collected on a Unico 4802 UV/vis double beam spectrophotometer. The scanning wavelength was from 200 nm to 1000 nm with a resolution of 1 nm.

2.3.2. ξ-Potential characterization

Zeta potential of dilute halloysite and chitosan–HNTs (1:1, weight ratio) suspensions (0.1 mg/ml) in aqueous solution, with pH adjustment using 0.1 M HCl or 0.1 M NaOH, was measured using a Zetasizer Nano ZS (Malvern Ltd., UK). Prior to each measurement, the operating conditions were checked and adjusted using a calibrated latex dispersion supplied by the instrument manufacturer (zeta potential -50 ± 5 mV).

2.3.3. Atomic force microscopy (AFM)

To evaluate the nanotopographic features and the surface morphology of pure chitosan and chitosan/HNTs nanocomposite films, a multimode AFM with NanoScope IIIa controller was used (Veeco Instruments). Measurements were performed in contact mode under ambient conditions using silicon tips.

2.3.4. Fourier transform infrared spectroscopy (FTIR)

The FTIR spectra of pure chitosan and chitosan/HNTs nanocomposites films were measured using attenuated total reflectance (ATR) model in a Bruker FTIR. ATR was a sampling technique used in conjunction with infrared spectroscopy which enables samples to be examined directly in the solid or liquid state without further preparation. Thirty-two consecutive scans were taken and their average was stored. Spectra were taken from 4000 to 400 cm^{-1}. The resolution of the wavenumber was 2 cm^{-1}.

2.3.5. Tensile properties test

The chitosan and chitosan/HNTs nanocomposite films were cut into the dog-bone shape firstly and then were stretched at 5 mm/min rate using Zwick/Roell Z005 machine. The stress–strain curves for every sample were recorded. At least five specimens for every sample were tested for reliable data. The value of the Young's modulus was obtained in the strain range of 0.1–0.25% according to the standard of ASTM E111-97 and JB/T 6544-93 (China). And the data was automatically given by the software of the machine.

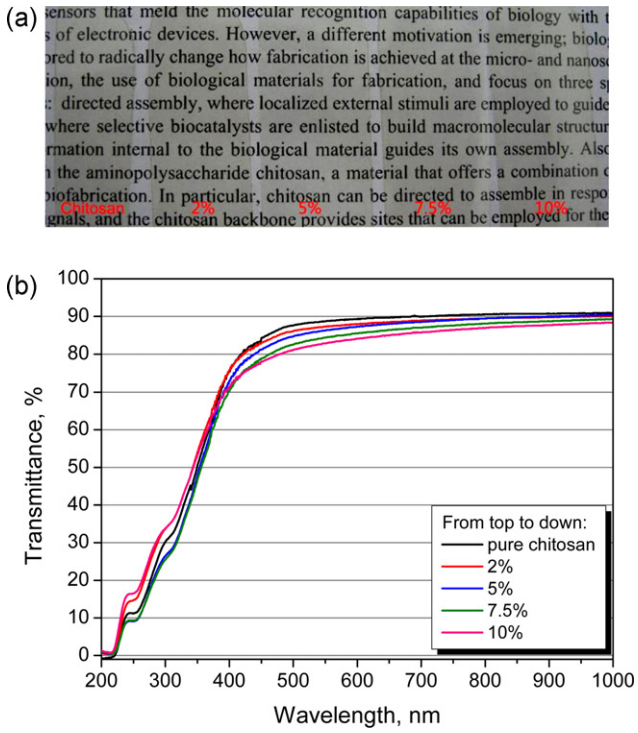

Fig. 1. Appearance (a) and UV–vis spectra (b) of the chitosan and chitosan/HNTs nanocomposite films.

2.3.6. Dynamic mechanical analysis (DMA)

Dynamic mechanical analyses of pure chitosan and chitosan/HNTs nanocomposite films were conducted with a NETZSCH Instruments DMA 242 at an oscillation frequency and heating rate of 1.0 Hz and 5 °C/min, respectively. The tensile mode was selected and the experiment was conducted at a temperature range of 40–210 °C in air atmosphere.

2.3.7. Scanning electron microscopy (SEM)

The morphology of nanocomposites was investigated by field emission scanning electron microscopy (FE-SEM) using an LEO1530 VP SEM machine operated at an acceleration voltage of 5 kV. The micrographs were taken from the surface of cryofractured samples previously coated with gold.

2.4. In vitro fibroblasts response on pure chitosan and chitosan/HNTs nanocomposite films

2.4.1. Cell culture

All films were treated with 2 wt.% sodium hydroxide aqueous solution to remove excessive acetic acid, then rinsed with a good deal of distilled water and dried at 40 °C. Prior to cell culture assays, all the films were sterilized by exposure to UV light for 30 min and washed by phosphate buffer saline solution (PBS) for three times. NIH3T3 mouse fibroblast cell line used in the experiments was passages 5. Cells were cultured and passaged in regular culture media consisting of Dulbecco's modified eagle medium (DMEM) supplemented with 10 vol.% fetal bovine serum (FBS) and antibiotics penicillin 100 units/mL and streptomycin 100 μL/mL. Cells were incubated at 37 °C in a 5% CO_2 incubator and the medium was changed every 3 days. Cells were routinely removed from tissue culture polystyrene (TCPS) dish with 0.25% trypsin–EDTA and plated on different substrates. The seeding cell densities of 96 well culture plates were 2.0×10^4 cell/mL.

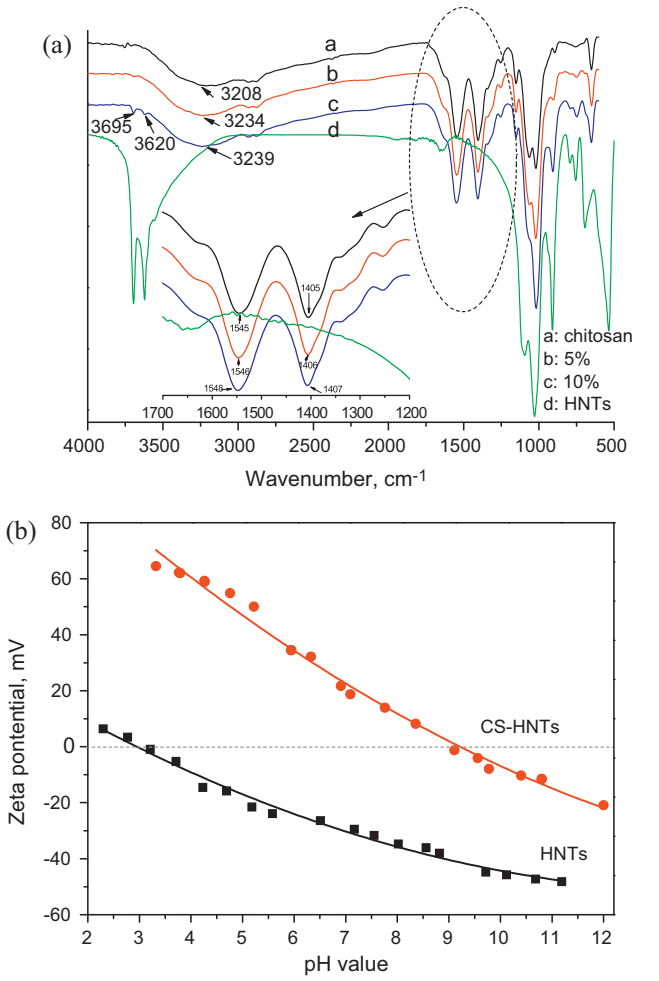

Fig. 2. Interactions between HNTs and chitosan: (a) FTIR of the pure chitosan, HNTs, and the chitosan/HNTs nanocomposites films; (b) zeta-potential plot for HNTs and chitosan–HNTs.

2.4.2. Optical cell morphology

All films remained fully transparent, which allowed a direct observation of cell morphology through the materials by an inverted phase contrast microscope. For assessing cell morphology, the random images of cells on each substratum were acquired using a CCD camera after culturing 1 day, 3 day and 7 day in regular media.

2.4.3. Scanning electron microscopy (SEM)

SEM analyses were performed to study the morphology of the cells grown on the surface of the pure chitosan and chitosan/HNTs nanocomposite films. At the third day, the medium was removed and the wells were washed twice with PBS. The cells were then fixed with 2.5% glutaraldehyde in cacodylate buffer (Karnovsky fixation solution) for 24 h at 4 °C. Then, the specimens were washed with cacodylate buffer several times and the dehydration of the cells attached to the films were done in ethanol at 30, 50, 70, 80, 90, 95 and 100%, immersed for 15 min at each step. Then all the samples were freeze-dried at −80 °C. A 10 nm thick gold–palladium layer was deposited on the samples with the use of a sputter coater (BALTEC SCD 005). The morphologies of the cells attached to the surfaces of chitosan and chitosan/HNTs films were taken by a Philips XL30 ESEM.

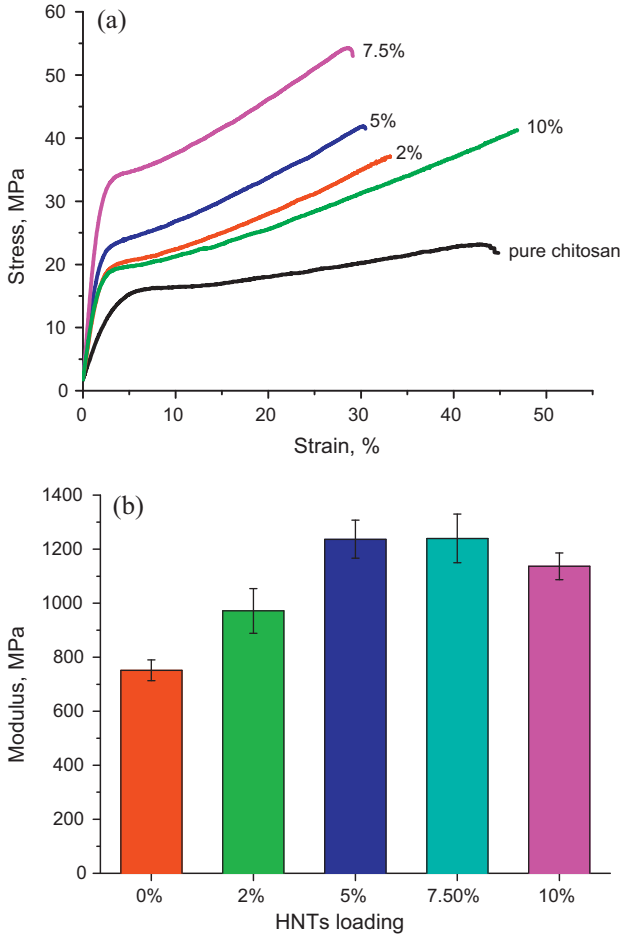

Fig. 3. Tensile property for the chitosan/HNTs nanocomposite films: (a) stress–strain curves; (b) Young's modulus.

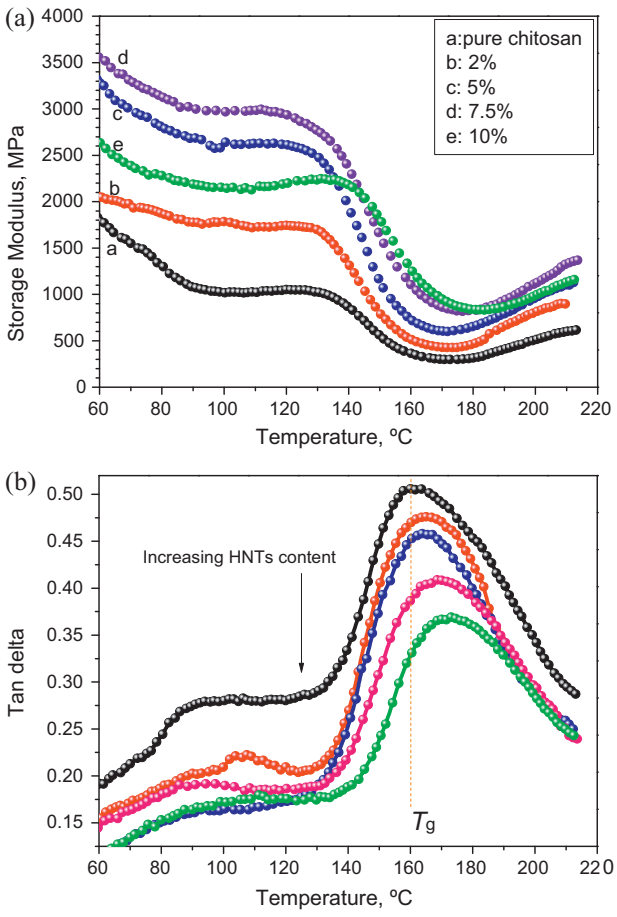

Fig. 4. Storage modulus (a) and tan δ (b) *vs.* temperature curves for chitosan/HNTs nanocomposite films.

2.4.4. Cell viability assay

Cell proliferation on the pure chitosan and chitosan/HNTs nanocomposite films was assessed by dimethylthiazol diphenyl tetrazolium bromide (MTT) assay. Cells were seeded at a density of 2×10^3 cells/well onto the equilibrated membranes in 96-well cell culture plates and were incubated at 37 °C in 5% CO_2 incubator. At the time point of 1, 3, 7 days, 10 μL MTT solution (5 mg/mL) was added to each well. After incubation for 4 h at 37 °C, the upper medium was removed carefully and the intracellular formazan was dissolved by adding 100 μL dimethyl sulfoxide (DMSO) to each well. Then the solutions were jolted by a shaker for 15 min. The absorbance was measured at 570 nm using the spectrophotometric microplate reader (Bio-Rad, Model 680, USA). Experiments were run in triplicate per sample. The cells inoculated directly on TCPS were regarded as a negative control. All data were expressed as the mean ± standard deviation (SD) for $n = 3$. The difference among individual groups was evaluated by the Student's *t*-test, with a *p*-value less than 0.05 being considered significantly different.

3. Results and discussion

3.1. Interaction between HNTs and chitosan

Chitosan is a natural polycationic biopolymer that can be dissolved in diluted aqueous acetic acid solution. Due to the protonation of the amines at low pH (less than 6), the chitosan is positively charged in the solution. The HNTs are negatively charged surface due to isomorphous substitution of Al^{3+} for Si^{4+} [22]. Therefore, mixing chitosan with HNTs in acid aqueous solution could result in the electrostatic attraction between them. On the other hand, the amine groups and hydroxyl groups on the chitosan can interact with the Si—O bonds of HNTs *via* hydrogen bonding interactions. It can be assumed that the nanotubes can be warped by chitosan chains due to the two types of interactions. Therefore, HNTs–chitosan hybrid can be formed in the solution. Hybrids of clays and chitosan *via* the electrostatic and hydrogen bonding interactions have been suggested [38–40].

We prepared pure chitosan and nanocomposite films in acetic acid solutions (pH value is around 4.0) at room temperature, since both the chitosan and HNTs is stable in this condition. In concentrated acid or alkaline solutions, HNTs can alter its chemical composition and morphology significantly [41]. While in dilute acid and alkaline solutions at room temperature, HNTs is stable. Increasing of the pH value above 6.5, chitosan is not soluble and will precipitate from the systems. This affects the homogenous of the nanocomposites. If preparing the films at low pH, the degradation of the backbone of chitosan can occur quickly. As a result, decreased strength of the films will be predicted. Fig. 1(a) shows the appearance of pure chitosan and chitosan/HNTs nanocomposite films. It can be seen that all films are transparent and HNTs nearly do not affect the light transmittance of chitosan even when the loading of HNTs is 10%. This indicates that the individual HNTs particles do not form aggregates [34]. Fig. 1(b) compares the UV/vis spectra for pure chitosan and chitosan/HNTs nanocomposite films. The films are strongly absorbing in the UV region of the spectrum (below 400 nm) due to the presence of absorbing entities for both HNTs and chitosan. We mainly focus on the visible region where we can compare

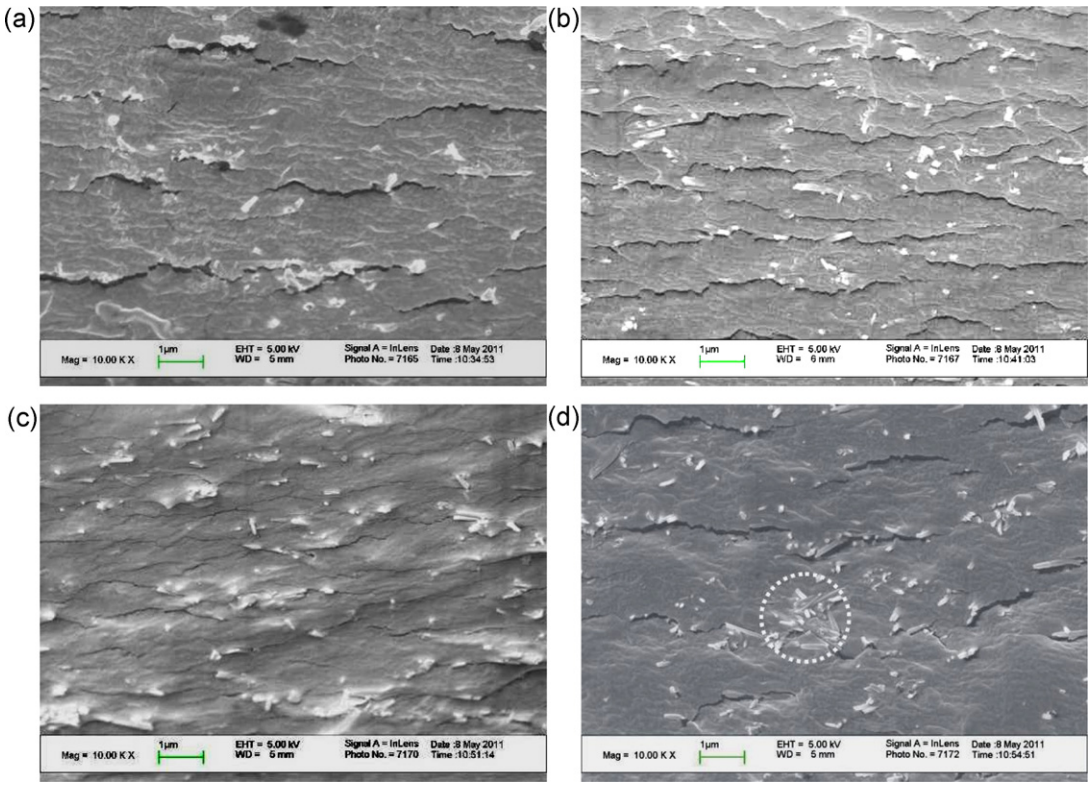

Fig. 5. SEM photos of the fracture surfaces of the chitosan/HNTs nanocomposite with 2% (a), 5% (b), 7.5% (c), and 10% (d) HNTs (the white circle region represents the HNTs aggregates).

the transparency of pure chitosan film with the nanocomposite films. Since the human eye has the highest sensitivity at 550 nm, the spectra of samples were compared with respect to their transmission at this wavelength. All films show above 80% transparency across the visible light spectrum (400–1000 nm). The transmittance through the nanocomposites with different HNTs contents is less 6%. This can be explained by that nano-scaled HNTs are dispersed uniformly in the chitosan matrix which is originated from the interfacial interactions between HNTs and chitosan. Other HNTs based biopolymer nanocomposites are also close to transparency due to the strong interfacial interactions and uniform dispersion of HNTs [34,37].

To investigate the interactions between HNTs and chitosan, FTIR spectra for the pure chitosan and chitosan/HNTs bionanocomposite films were compared. As shown in Fig. 2(a), in the spectrum of chitosan, there are two characteristic peaks at 1545 cm^{-1} and 1405 cm^{-1}, which correspond to the deformation vibration of the protonated amine group ($-NH_3^+$) and hydroxyl group respectively [42,43]. The two peaks for the chitosan/HNTs nanocomposites slightly shift to higher frequencies (*i.e.* the absorbance band of NH_2 vibration moves from 1545 to 1548 cm^{-1} for the nanocomposites with 10% HNTs) due to the electrostatic interactions and H-bonding interaction between nanotubes and chitosan. On the other hand, the broad peaks around 3208 cm^{-1} of chitosan, which is attributed to the overlapped N—H band and O—H band vibration, also moves to higher frequencies in the nanocomposites. For example, the nanocomposites with 10% HNTs show the peak around 3239 cm^{-1}. Formation of hydrogen bonding can induce the blue-shift or red-shift of the IR absorbance in different systems. This can be explained by the different changes of electron density distribution of atoms involved in the hydrogen bonding [44]. All the changes in IR spectrum suggest the interactions between HNTs and chitosan *via* the electrostatic interaction and hydrogen bonding. In addition, two peaks around 3620 cm^{-1} and 3695 cm^{-1} appears in the spectrum of the nanocomposites with relatively higher HNTs loading, which are attributed to the Al_2—OH stretching bands of HNTs [22]. This demonstrates that HNTs are exposed on the nanocomposite surfaces.

Zeta potential measurements were further performed to investigate the interactions between HNTs and chitosan. Fig. 2(b) shows the curves for halloysite and chitosan over a wide pH range. It is apparent from the plots that the surface charge of the HNTs is only slightly positive at very low pH. As the pH value increases from 2 to 12, the surface charge falls sharply to reach a negative value. The negatively charged HNTs is related to the silica groups located on their outer surfaces [23,45]. However, after complexation with chitosan, the chitosan–HNTs hybrid shows a positive potential over the pH range of 3–9. For instance, the zeta potential value of chitosan–HNTs hybrid at pH 6 is 34.5 mV. This suggests that the positively charged chitosan can warp the tubes *via* the electrostatic attraction interactions in the acidic aqueous solution. Chitosan–HNTs hybrid becomes negative charged when the pH is higher than 9. This is because that pH value substantially alters the charged state and properties of chitosan. At low pH, the amines of chitosan are protonated and positively charged, and chitosan is a water-soluble cationic polyelectrolyte. At high pH, chitosan's amines become deprotonated and the polymer loses its charge and becomes insoluble [3]. Chitosan will gradually precipitate from the systems. So the zeta-potential of chitosan–HNTs is close to HNTs at higher pH.

3.2. Mechanical properties of the chitosan/HNTs nanocomposite films

HNTs are natural 1D nanomaterials that could be used as nanofillers in different polymers. Due to the strong interfacial interactions between HNTs and chitosan, the chitosan/HNTs nanocomposites are expected to show improved mechanical

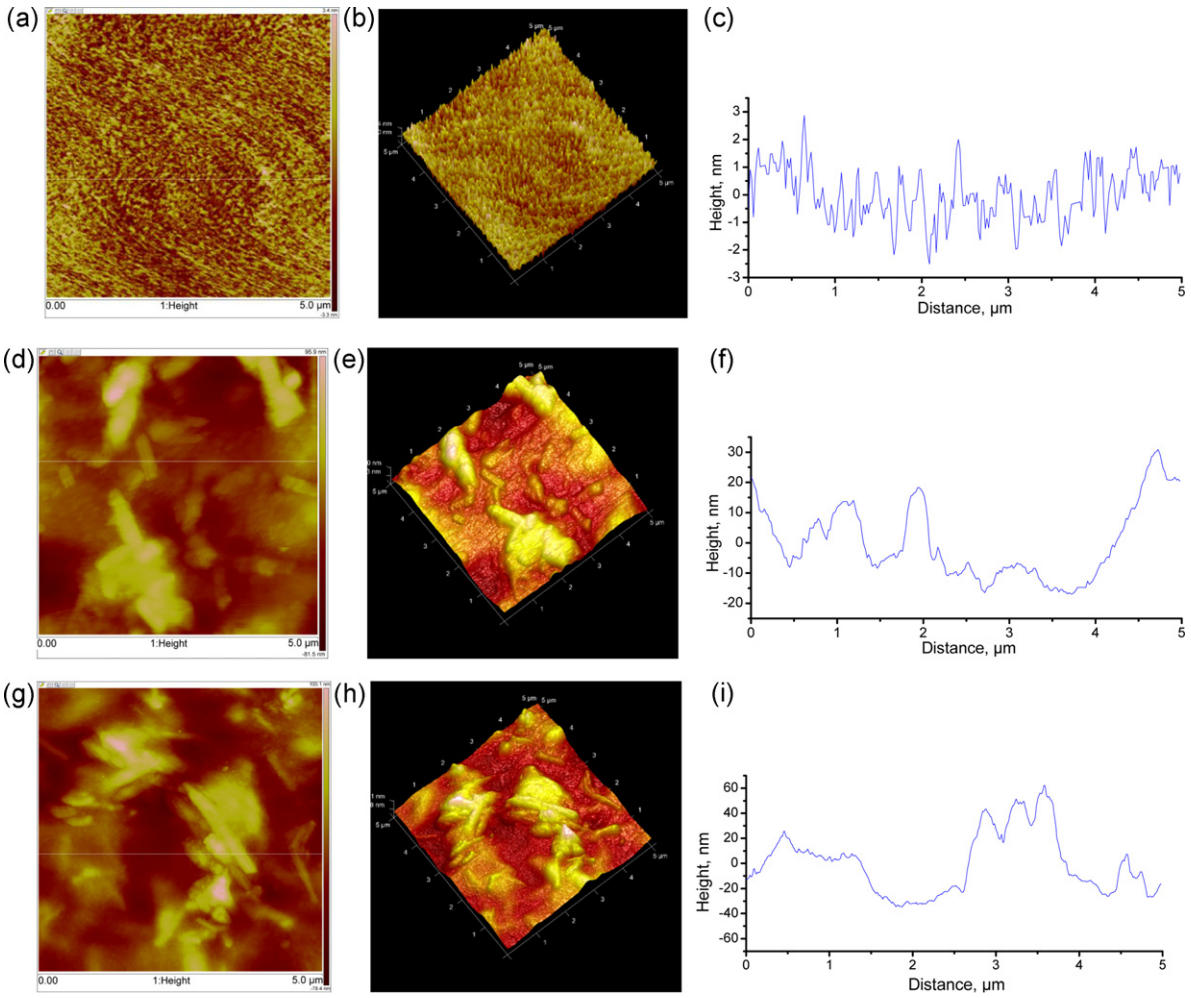

Fig. 6. AFM height images, 3D topography, and R_q profile of the line scan of chitosan/HNTs nanocomposite films: (a)–(c) pure chitosan; (d)–(f) 5% HNTs; (g)–(i) 10% HNTs.

properties. The influence of HNTs on the tensile properties of chitosan film was firstly investigated. As shown in Fig. 3, HNTs significantly improve both tensile strength and Young's modulus of chitosan film. These mechanical properties of the nanocomposites are improved with the loading of HNTs up to 7.5%. For example, the tensile strength and tensile modulus for chitosan/HNTs nanocomposites with 7.5% HNTs are 54.2 MPa and 1240 MPa, which are 134% and 65% higher than those of the pure chitosan respectively. The elongation at break is slightly decreased for the nanocomposites compared with the pure chitosan, indicating the toughness of the chitosan is partly sacrificed with the incorporation of HNTs. This agrees with most of particles filled polymer systems, as the strength and toughness of materials always have trade-off relationship [46]. The slightly decreased strength and modulus of composites with higher HNTs content (above 7.5%) are correlated to the presence of HNTs aggregates in the composites (SEM result below). The HNTs aggregates could serve as stress concentration points. Nevertheless, their strength and modulus are still higher than those properties of pure chitosan. The reinforcing effects of nanoparticle for polymers are related to the dispersion state of nanoparticles in the matrix and their interfacial interactions [46]. Raw HNTs exhibit good reinforcing ability for the chitosan in term of the mechanical properties. The reinforcing effect of HNTs on chitosan could be attributed to (i) the interactions between HNTs and the chitosan as shown in the IR and Zeta potential results and (ii) the uniformly distributed rigid nanotubes in chitosan matrix (SEM result below). But, HNTs causes deterioration in tensile strength and elongation at break of pectins films, although HNTs also show good dispersion and can interact with the pectins [34]. The different reinforcing ability of HNTs for chitosan and pectins films may arise from the morphology difference of the nanotubes. In their work, the used HNTs bought from Aldrich show a low tubular quality, characteristic of high irregularity in diameter, wall thickness and morphology. In the present work, the used HNTs are mined from Hunan province

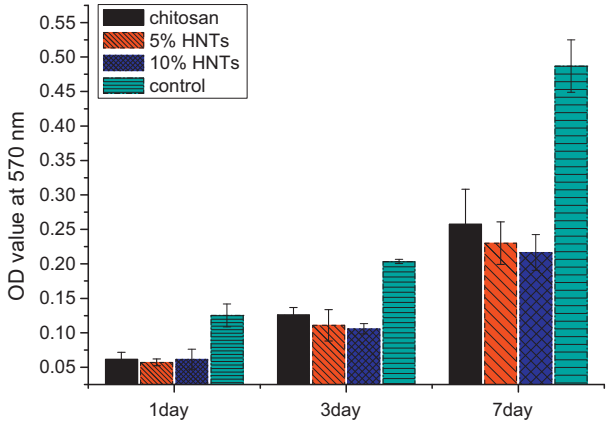

Fig. 7. MTT viability assay of NIH3T3 cells after 1, 3 and 7 day cell culture on pure chitosan and chitosan/HNTs bionanocomposite films in comparison with tissue culture PS (control).

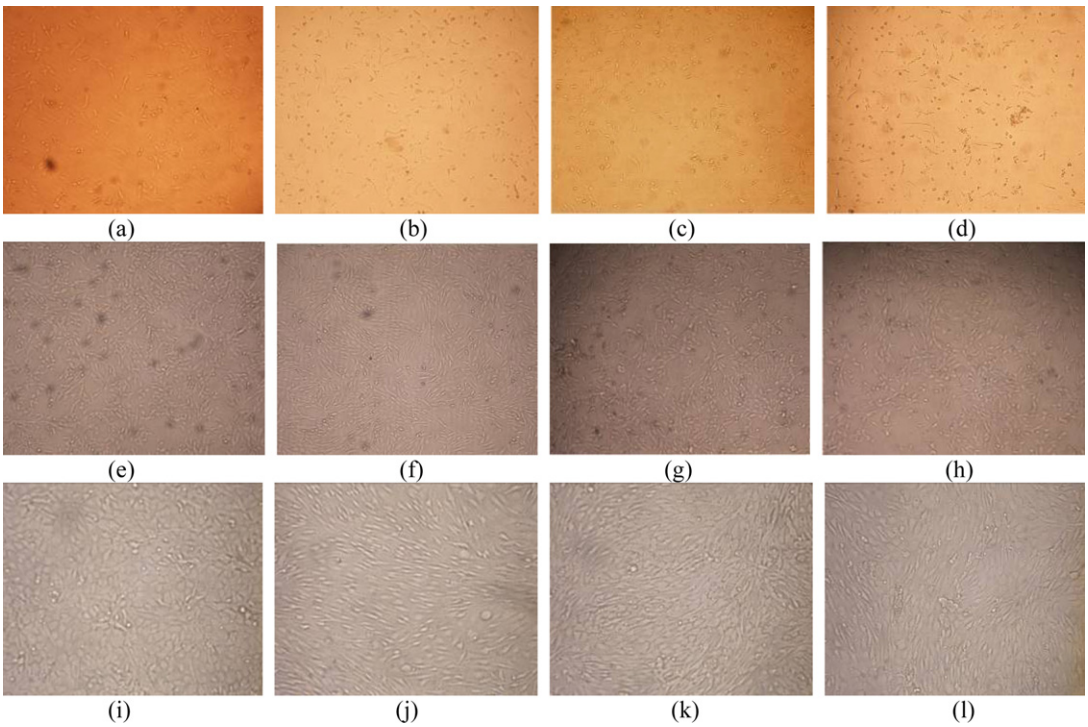

Fig. 8. Light microscopic images of fibroblast (NIH3T3) after 1 day, 3 day and 7 day on TCPS (a, e, and i), pure chitosan (b, f, and j), chitosan/HNTs with 5% HNTs (c, g, and k), and chitosan/HNTs with 10% HNTs (d, h, and l) bionanocomposite film.

of China, which show a high relatively uniform morphology with good tubular quality [27].

To further illustrate the effect of HNTs on the mechanical properties of chitosan film, DMA experiment was conducted. The dynamic modulus and tan δ spectra of pure chitosan and chitosan/HNTs nanocomposite films are compared in Fig. 4. From the figure, in the test temperature range, the modulus of the nanocomposite films increase with the increase of HNTs content until the loading of HNTs of 7.5%, suggesting the reinforcing effect of HNTs to chitosan. Since HNTs are inorganic rigid silicate nanotubes with high aspect ratio and interfacial reactions taking place between HNTs and chitosan, the chitosan/HNTs nanocomposite films show higher modulus at glassy state and rubbery state. For example, the storage modulus of the nanocomposite with 7.5% HNTs at 100 °C and 200 °C is 193% and 119% higher than those of pure chitosan respectively. Apart from the increased storage modulus, the glass transition temperatures of chitosan also increase by HNTs as shown in Fig. 4(b). It can be seen all the samples show a transition peak in the temperature range of 130–210 °C, which is related to the glass transition of the chitosan matrix. The temperature at the peak of tan δ curve is assigned to the glass transition temperature (T_g) of the polymers. The T_g of the nanocomposites increases consistently with the increase in loading of HNTs. The maximum T_g of the nanocomposites is 172 °C for the composites with 10% HNTs, which is 12 °C higher than that of pure chitosan. In addition, the intensity of the loss tangent (tan δ) peaks for nanocomposites is lower than that of pure chitosan, as the chitosan can dissipates more energy applied to the sample due to its viscous response at high temperature. For polymer nanocomposites, when there are wetted interfaces but no significant attractive interfacial interactions, the T_g is equal to neat, bulk T_g. When the interface is non-wetted, that is, when a free surface is present between the polymer and the nanofiller, there is a reduction in T_g relative to neat, bulk T_g. When the nanofillers possess either attractive interactions or covalent bonding to the polymer, the T_g of the polymer is increased relative to neat, bulk T_g [47,48]. Therefore, the increased T_g of chitosan by HNTs can be attributed to the strong interfacial interactions as illustrated by the FTIR and Zeta-potential results above. If chitosan just mixed with nanoparticles but without interactions, the T_g of chitosan could not change.

3.3. Morphology of the chitosan/HNTs nanocomposite films

Assessment of the dispersion state of HNTs in the chitosan matrix is essential to understand the nanocomposite behavior. As shown in Fig. 5, all SEM micrographs show that HNTs with tubular structure are uniformly dispersed in the matrix and the interface between HNTs and chitosan matrix is blurry. This can be attributed to the interfacial interactions between HNTs and chitosan as illustrated previously. The uniformly dispersed and rigid inorganic nanotubes can effectively absorb and dissipate the energy during the mechanical fracture. Therefore, chitosan/HNTs nanocomposites exhibit substantially improve mechanical and thermal performance compared with pure chitosan. When the loading of HNTs increase above 7.5%, the chitosan/HNTs nanocomposites show morphology of coexistence of both individually dispersed nanotubes and HNTs aggregates. From Fig. 5(d), HNTs aggregates are in about 1 μm × 1 μm, which consist of several nanotubes. The formation of HNTs aggregates in chitosan can be attributed to the re-aggregation of HNTs during drying process of the films due to the interactions among the tubes. The aggregated HNTs can act as the stress centered points. As a consequence, the nanocomposites show decreased tensile properties and storage modulus at higher HNTs loadings (10%). The re-aggregation of HNTs during evaporation of the solvent for the solution casting method has also been suggested in other systems [26].

3.4. Nanotopography of the chitosan/HNTs nanocomposite films

The surface nanotopography and toughness of pure chitosan and the nanocomposite were investigated by AFM. Fig. 6 compares the height image, 3D topography, and the line scan of the pure

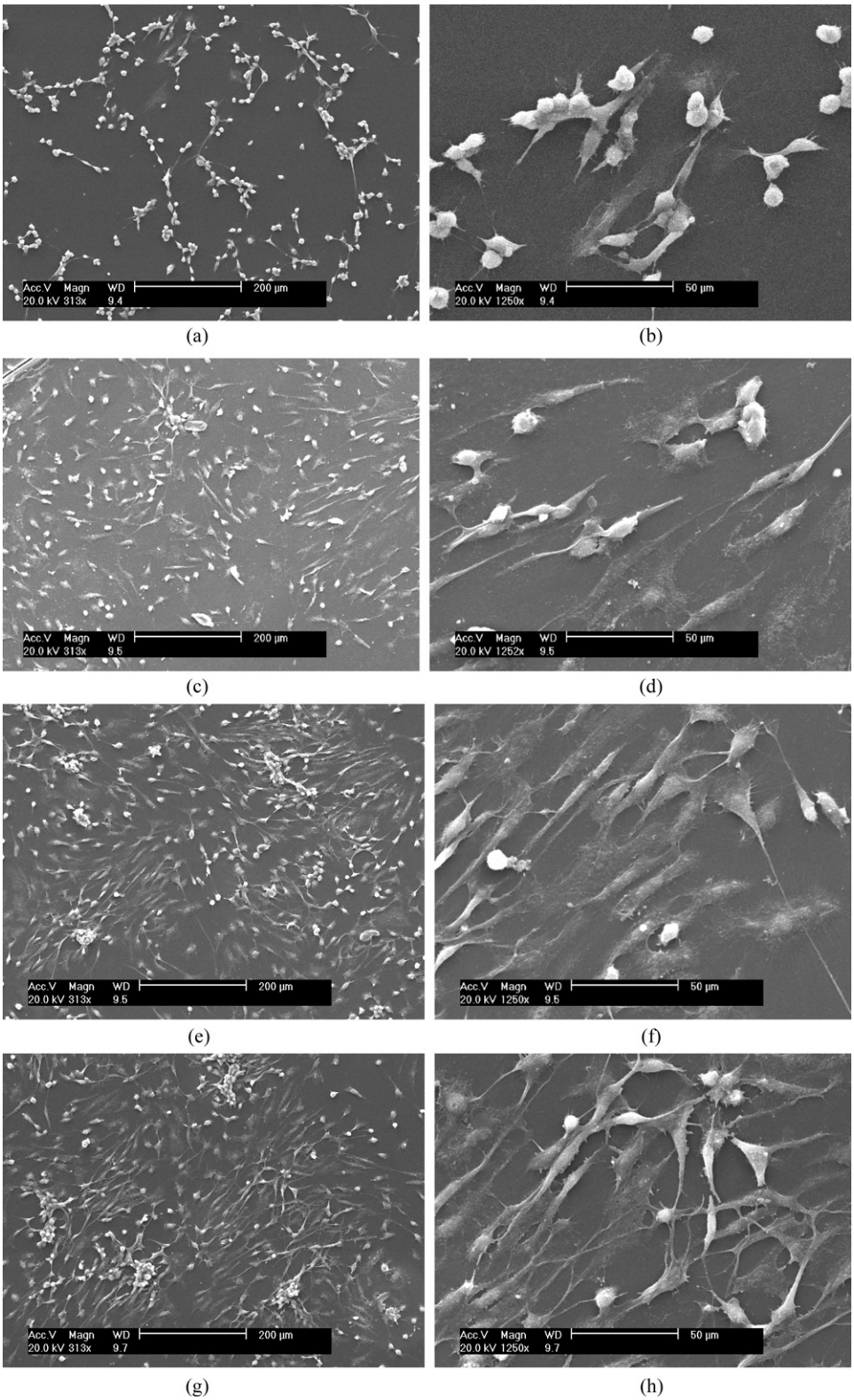

Fig. 9. SEM images of fibroblast (NIH3T3) cultured on TCPS (a and b), pure chitosan (c and d) and chitosan/HNTs with 5% HNTs (e and f) and chitosan/HNTs with 10% HNTs (g and h) bionanocomposite at day 3.

chitosan films and the nanocomposite films. From Fig. 6, it can be seen that pure chitosan films have smooth and uniform surface with uniformly dispersed nanopores. Nanopores in the chitosan film are formed by water evaporation during the drying process of the films. In contrast, the nanocomposites films exhibit a substantial increase of surface roughness relative to the pure chitosan films and embedded HNTs in the matrix are found on these surfaces. Consistent with SEM results, when the loading of HNTs is relatively low, HNTs can be uniformly dispersed in the chitosan matrix. However, the HNTs aggregates of *ca.* 3 micron in size are

also been found on the surface of nanocomposites with higher HNTs loadings. HNTs aggregates may be formed during the drying process for these nanocomposite films [26]. From Fig. 6(c), the surface roughness of pure chitosan film is the range of 2–6 nm across the area. After incorporation of HNTs, the surface roughness is in the range of 20–50 nm and 70–120 nm for the nanocomposites with 5% HNTs and 10% HNTs, respectively. The presence of HNTs and its aggregates contributed to the increase in the surface roughness, as shown in Fig. 6. The surface roughness may play an important role in cell adhesion and proliferation, which will be illustrated below.

3.5. Biocompatibility of the chitosan/HNTs nanocomposite films

For issue engineering materials or drug carrier application, chitosan and chitosan/HNTs nanocomposites must be non-toxic and biocompatible. We utilized *in vitro* mouse NIH3T3 cell lines from cell banks to evaluate the cytotoxicity of chitosan and chitosan/HNTs nanocomposite films. The viability of NIH3T3 cells exposed to chitosan and chitosan/HNTs nanocomposites with different HNTs concentrations is summarized in Fig. 7. The results reveal that 3T3 cells can adhere and proliferate on both pure chitosan and chitosan/HNTs nanocomposite. With increasing culturing time, the absorbance for all the samples increases, indicating the well growth of the cells. No visible reduction in viability between the chitosan and chitosan/HNTs nanocomposite can be found at 1, 3 and 7 days culture. In view of the non-significant variances ($p < 0.05$) between these samples, chitosan/HNTs nanocomposites show comparable biocompatibility with pure chitosan. Consistent with previous report, HNTs based polymer composites are noncytotoxicity to various cells [23,35,37], which suggests that HNTs have good cytocompatibility. However, the OD values of both pure chitosan and the chitosan/HNTs nanocomposites are lower than the control (TCPS) especially after 7 days culture. This possibly may be attributed to the more hydrophobic character of TCPS compared with chitosan and nanocomposite films, as cell adhesion proteins tend to bind the hydrophobic surface. The decreased cell viability of chitosan surface compared with the TCPS has also been reported [16]. Fig. 8 shows the optical micrographs of 3T3 cells after culture at 1 day, 3 day and 7 day on pure chitosan and the nanocomposites. Fibroblast cells began to display round or fusiform shape on the surfaces of both pure chitosan and chitosan/HNTs nanocomposites as early as 24 h after seeding, indicating that the cell can be attached on these materials. It can be seen that fibroblasts attached on all the surfaces changed their original shape to fusiform shape after cultured for three days. Cells continue to proliferate on the surfaces for all the samples and become subconfluent on the 7th day of culture. The phenotype and interaction of cells on the surfaces of the samples were further evaluated using morphological techniques. Fig. 9 represents the SEM micrographs of fibroblasts cultured for 3 days on TCPS, pure chitosan and chitosan/HNTs nanocomposite films. It can be seen that fibroblasts attached on all the surfaces changed their original shape to fusiform shape after cultured for three days. The cells grown on both chitosan and chitosan/HNTs nanocomposite films show well-expanded in typical spindle morphologies and forming intercellular tight junctions with adjacent cells. There is a slight difference in cell morphology among the cells grown on pure chitosan film and the nanocomposite films. The cell surfaces tend more flat on chitosan/HNTs nanocomposite compared with pure chitosan. This may be attributed to the much higher roughness for the nanocomposite surfaces. At high magnification SEM image, the cells are anchored to substrate surfaces by discrete filopodia exhibiting numerous microvilli. In general, the cell behavior is related to the nanotopography features and surface chemistry of the bioactive materials. The increased surface roughness and the presence of Si element in the chitosan/HNTs nanocomposite surface are beneficial to attachment of the cells [37,49]. From the MTT assay and morphology results, it should be concluded that HNTs has little influence on the cytocompatibility of chitosan. The chitosan/HNTs nanocomposites are biocompatible materials, which can be used as cell culture scaffold.

4. Conclusions

Naturally occurred HNTs were incorporated into chitosan for forming bionanocomposite films *via* solution casting. The electrostatic attraction and hydrogen bonding interactions between HNTs and chitosan were confirmed. HNTs were uniformly dispersed in the chitosan matrix. The tensile properties of chitosan were enhanced by HNTs significantly. The storage modulus and glass transition temperature of chitosan/HNTs films were also increased significantly with HNTs. The incorporation of HNTs induced changes in surface nanotopography of chitosan and lead to the increased roughness of the nanocomposite films. NIH3T3 cells can adhere to and develop on the chitosan/HNTs bionanocomposite films as well as on pure chitosan film. Chitosan/HNTs were cytocompatibility even when the loading of HNTs was 10%. These results provided insights into the understanding of structural relationships of chitosan/HNTs bionanocomposite films in potential applications, such as scaffold materials in tissue engineering.

Acknowledgements

This work was financially supported by the Research Fund for the Doctoral Program of Higher Education of China (grant no. 20114401120003), Key Laboratory of Rubber-plastics (Qingdao University of Science and Technology), Ministry of Education and the Key Laboratory of High Performance and Functional Polymeric Materials (South China University of Technology), Guangdong province, PR of China. The authors also thank Dr. Hau-To Wong for proof reading of the manuscript.

References

[1] E. Khor, Chitin: Fulfilling a Biomaterials Promise, Elsevier Science, 2001.
[2] N.V. Majeti, R. Kumar, Reactive and Functional Polymers 46 (2000) 1–27.
[3] H. Yi, L.-Q. Wu, W.E. Bentley, R. Ghodssi, G.W. Rubloff, J.N. Culver, G.F. Payne, Biomacromolecules 6 (2005) 2881–2894.
[4] M. Dash, F. Chiellini, R.M. Ottenbrite, E. Chiellini, Progress in Polymer Science 36 (2011) 981–1014.
[5] M. Wang, Biomaterials 24 (2003) 2133–2151.
[6] P. Kithva, L. Grndahl, D. Martin, M. Trau, Journal of Materials Chemistry 20 (2010) 381–389.
[7] X. Wang, Y. Du, J. Luo, B. Lin, J.F. Kennedy, Carbohydrate Polymers 69 (2007) 41–49.
[8] M. Lavorgna, F. Piscitelli, P. Mangiacapra, G.G. Buonocore, Carbohydrate Polymers 82 (2010) 291–298.
[9] S.-F. Wang, L. Shen, W.-D. Zhang, Y.-J. Tong, Biomacromolecules 6 (2005) 3067–3072.
[10] C. Tang, L. Xiang, J. Su, K. Wang, C. Yang, Q. Zhang, Q. Fu, Journal of Physical Chemistry B 112 (2008) 3876–3881.
[11] J. Diaz-Visurraga, M.F. Melendrez, A. Garcia, M. Paulraj, G. Cardenas, Journal of Applied Polymer Science 116 (2010) 3503–3515.
[12] H. Fan, L. Wang, K. Zhao, N. Li, Z. Shi, Z. Ge, Z. Jin, Biomacromolecules 11 (2010) 2345–2351.
[13] X. Yang, Y. Tu, L. Li, S. Shang, X.-M. Tao, ACS Applied Materials and Interfaces 2 (2010) 1707–1713.
[14] X. Wang, Y. Tang, Y. Li, Z. Zhu, Y. Du, Journal of Biomaterials Science Polymer Edition 21 (2010) 171–184.
[15] M. Darder, M. Colilla, E. Ruiz-Hitzky, Applied Clay Science 28 (2005) 199–208.
[16] K.S. Katti, D.R. Katti, R. Dash, Biomedical Materials 3 (2008) 034122.
[17] M.-Y. Chang, R.-S. Juang, Journal of Colloid and Interface Science 278 (2004) 18–25.
[18] X. Wang, Y. Du, J. Luo, Nanotechnology 19 (2008) 065707.
[19] X. Wang, Y. Du, J. Luo, J. Yang, W. Wang, J.F. Kennedy, Carbohydrate Polymers 77 (2009) 449–456.
[20] S.F. Wang, L. Shen, Y.J. Tong, L. Chen, I.Y. Phang, P.Q. Lim, T.X. Liu, Polymer Degradation and Stability 90 (2005) 123–131.
[21] P. Monvisade, P. Siriphannon, Applied Clay Science 42 (2009) 427–431.

[22] E. Joussein, S. Petit, J. Churchman, B. Theng, D. Righi, B. Delvaux, Clay Minerals 40 (2005) 383–426.
[23] V. Vergaro, E. Abdullayev, Y.M. Lvov, A. Zeitoun, R. Cingolani, R. Rinaldi, S. Leporatti, Biomacromolecules 11 (2010) 820–826.
[24] M.L. Du, B.C. Guo, D.M. Jia, Polymer International 59 (2010) 574–582.
[25] Y.P. Ye, H.B. Chen, J.S. Wu, L. Ye, Polymer 48 (2007) 6426–6433.
[26] M. Liu, B. Guo, M. Du, D. Jia, Applied Physics A 88 (2007) 391–395.
[27] M.X. Liu, B.C. Guo, M.L. Du, X.J. Cai, D.M. Jia, Nanotechnology 18 (2007) 455703.
[28] B.C. Guo, Q.L. Zou, Y.D. Lei, M.L. Du, M.X. Liu, D.M. Jia, Thermochimica Acta 484 (2009) 48–56.
[29] M.X. Liu, B.C. Guo, Q.L. Zou, M.L. Du, D. Jia, Nanotechnology 19 (2008) 205709.
[30] M.L. Du, B.C. Guo, Y.D. Lei, M.X. Liu, D.M. Jia, Polymer 49 (2008) 4871–4876.
[31] X. Sun, Y. Zhang, H. Shen, N. Jia, Electrochimica Acta 56 (2010) 700–705.
[32] I.P. Dobrovol'skaya, P.V. Popryadukhin, A.Y. Khomenko, E.N. Dresvyanina, V.E. Yudin, V.Y. Elokhovskii, S.N. Chvalun, N.N. Saprykina, T.P. Maslennikova, E.N. Korytkova, Polymer Science, Series A. Polymer Physics 53 (2011) 418–423.
[33] Y. Zheng, A. Wang, Journal of Macromolecular Science Pure and Applied Chemistry 47 (2010) 33–38.
[34] G. Cavallaro, G. Lazzara, S. Milioto, Langmuir 27 (2011) 1158–1167.
[35] R. Qi, R. Guo, M. Shen, X. Cao, L. Zhang, J. Xu, J. Yu, X. Shi, Journal of Materials Chemistry 20 (2010) 10622–10629.
[36] R. Qi, M. Shen, X. Cao, R. Guo, X. Tian, J. Yu, X. Shi, Analyst 136 (2011) 2897–2903.
[37] W.Y. Zhou, B. Guo, M. Liu, R. Liao, A.B.M. Rabie, D. Jia, Journal of Biomedical Materials Research Part A 93A (2009) 1574–1587.
[38] M. Darder, M. Colilla, E. Ruiz-Hitzky, Chemistry of Materials 15 (2003) 3774–3780.
[39] H.-B. Yao, Z.-H. Tan, H.-Y. Fang, S.-H. Yu, Angewandte Chemie International Edition 49 (2010) 10127–10131.
[40] M. Darder, M. Lopez-Blanco, P. Aranda, A.J. Aznar, J. Bravo, E. Ruiz-Hitzky, Chemistry of Materials 18 (2006) 1602–1610.
[41] R.D. White, D.V. Bavykin, F.C. Walsh, Nanotechnology 23 (2012) 065705.
[42] A. Pawlak, M. Mucha, Thermochimica Acta 396 (2003) 153–166.
[43] W. Tan, Y. Zhang, Y.-S. Szeto, L. Liao, Composites Science and Technology 68 (2008) 2917–2921.
[44] J. Joseph, E.D. Jemmis, Journal of the American Chemical Society 129 (2007) 4620–4632.
[45] S.R. Levis, P.B. Deasy, International Journal of Pharmaceutics 243 (2002) 125–134.
[46] A. Okada, A. Usuki, Macromolecular Materials and Engineering 291 (2006) 1449–1476.
[47] K.J. Lee, D.K. Lee, Y.W. Kim, W.-S. Choe, J.H. Kim, Journal of Polymer Science Part B: Polymer Physics 45 (2007) 2232–2238.
[48] D.R. Paul, L.M. Robeson, Polymer 49 (2008) 3187–3204.
[49] D.S. Kommireddy, I. Ichinose, Y.M. Lvov, D.K. Mills, Journal of Biomedical Nanotechnology 1 (2005) 286–290.